Iron fertilization enhanced net community production but not downward particle flux during the Southern Ocean iron fertilization experiment LOHAFEX

Patrick Martin,[1,2] Michiel Rutgers van der Loeff,[3] Nicolas Cassar,[4] Pieter Vandromme,[5,6] Francesco d'Ovidio,[7] Lars Stemmann,[5] R. Rengarajan,[8] Melena Soares,[9] Humberto E. González,[10] Friederike Ebersbach,[3] Richard S. Lampitt,[1] Richard Sanders,[1] Bruce A. Barnett,[4] Victor Smetacek,[3] and S. Wajih A. Naqvi[9]

Received 12 June 2012; revised 24 July 2013; accepted 1 August 2013.

[1] A closed eddy core in the Subantarctic Atlantic Ocean was fertilized twice with two tons of iron (as $FeSO_4$), and the 300 km^2 fertilized patch was studied for 39 days to test whether fertilization enhances downward particle flux into the deep ocean. Chlorophyll *a* and primary productivity doubled after fertilization, and photosynthetic quantum yield (F_V/F_M) increased from 0.33 to ≥0.40. Silicic acid (<2 μmol L^{-1}) limited diatoms, which contributed <10% of phytoplankton biomass. Copepods exerted high grazing pressure. This is the first study of particle flux out of an artificially fertilized bloom with very low diatom biomass. Net community production (NCP) inside the patch, estimated from O_2:Ar ratios, averaged 21 mmol POC m^{-2} d^{-1}, probably ±20%. ^{234}Th profiles implied constant export of ~6.3 mmol POC m^{-2} d^{-1} in the patch, similar to unfertilized waters. The difference between NCP and ^{234}Th-derived export partly accumulated in the mixed layer and was partly remineralized between the mixed layer and 100 m. Neutrally buoyant sediment traps at 200 and 450 m inside and outside the patch caught mostly <1.1 mmol POC m^{-2} d^{-1}, predominantly of fecal origin; flux did not increase upon fertilization. Our data thus indicate intense flux attenuation between 100 and 200 m, and probably between the mixed layer and 100 m. We attribute the lack of fertilization-induced export to silicon limitation of diatoms and reprocessing of sinking particles by detritus feeders. Our data are consistent with the view that nitrate-rich but silicate-deficient waters are not poised for enhanced particle export upon iron addition.

Citation: Martin, P., et al. (2013), Iron fertilization enhanced net community production but not downward particle flux during the Southern Ocean iron fertilization experiment LOHAFEX, *Global Biogeochem. Cycles*, *27*, doi:10.1002/gbc.20077.

1. Introduction

[2] Iron limits primary productivity across large areas of the oceans, which hence contain perennially high NO_3^- and PO_4^{3-} stocks, but low chlorophyll *a* [*Boyd et al*., 2007]. Artificial Fe fertilization experiments (FeAXs) in these regions have induced blooms of large-celled diatoms, drawdown of macronutrients and fCO_2 in the surface mixed layer, and enhanced downward particle flux [*Boyd et al*., 2007; *Coale et al*., 2004; *de Baar et al*., 2005; *Smetacek et al*., 2012]. Analogous results are found in naturally iron-rich waters downstream of Southern Ocean islands [*Blain et al*., 2007; *Pollard et al*., 2009]. Ocean Fe fertilization has hence been proposed as a means to sequester CO_2 by increasing the downward flux of particulate organic carbon (POC), although the viability and side effects remain unclear [*Aumont and Bopp*, 2006; *Lampitt et al*., 2008a; *Lenton and Vaughan*, 2009; *Smetacek and Naqvi*, 2008; *Zeebe and Archer*, 2005]. Downward POC flux clearly influences atmospheric CO_2 [*Kwon et al*., 2009; *Parekh et al*., 2006], but we do not fully

Additional supporting information may be found in the online verson of this article.

[1]National Oceanography Centre, Southampton, UK.
[2]Now at Earth Observatory of Singapore, Singapore.
[3]Alfred Wegener Institute for Polar and Marine Research, Bremerhaven, Germany.

Corresponding author: P. Martin, Earth Observatory of Singapore, 50 Nanyang Ave., Singapore. (pmartin@ntu.edu.sg)

0886-6236/13/10.1002/gbc.20077

[4]Division of Earth and Ocean Sciences, Nicholas School of the Environment, Duke University, Durham, North Carolina, USA.
[5]LOV, Observatoire Océanologique, UMR7093, UPMC University of Paris 6, Villefranche/mer, France.
[6]Now at GEOMAR Helmholtz Centre for Ocean Research Kiel, Kiel, Germany.
[7]LOCEAN-IPSL, CNRS/IRD/UPMC/MNHN, Paris, France.
[8]Physical Research Laboratory, Ahmedabad, India.
[9]National Institute of Oceanography, Dona Paula, India.
[10]Instituto de Ciencias Marinas y Limnológicas, Universidad Austral de Chile, Valdivia, Chile.

understand the links between iron supply and POC flux and how they are influenced by planktonic community structure.

[3] Only two FeAXs were conducted in low-silicon (Si) waters (Southern Ocean iron enrichment experiment (SOFeX) North and SOLAS air-sea gas exchange experiment (SAGE)). However, diatoms were abundant and, apparently, not Si limited during SOFeX North [*Coale et al*., 2004], while downward particle export was not measured during SAGE [*Harvey et al*., 2010]. Recent work has suggested that Fe supply to low-Si Southern Ocean regions may not enhance POC flux, although appreciable POC flux occurs there naturally [*Bowie et al*., 2011; *Henson et al*., 2012; *Trull et al*., 2001a].

[4] It is important to note that the shallow export flux of POC, often measured at 100 m, generally does not sequester carbon from the atmosphere for climatically relevant time scales. Long-term sequestration requires POC to sink below the permanent thermocline, and it is this deeper flux that would need enhancing for geoengineering to work [*Lampitt et al*., 2008a]. POC flux can decrease sharply between these two depths, and the magnitude of this decrease depends on the community structure in the surface and mesopelagic [*Buesseler and Boyd*, 2009; *Boyd and Trull*, 2007; *Jacquet et al*., 2011; *Lam and Bishop*, 2007]. Enhancing POC export does not necessarily enhance POC sequestration, as heterotrophic activity in the mesopelagic might be stimulated [*Lomas et al*., 2010]. POC flux past the permanent thermocline must hence be measured during FeAXs, which so far has only been done in Si-rich waters [*Smetacek et al*., 2012].

[5] We measured production, export, and deep POC flux using multiple independent methods during LOHAFEX (*loha* is the Hindi word for iron), a 39 day FeAX in low-Si waters. We first present results from each method individually, examine the reasons for the lack of export, and, finally, discuss the depth horizons where and the processes by which flux was attenuated.

2. Methods

2.1. Site Selection, Fertilization, and Patch Tracking

[6] LOHAFEX was conducted aboard R/V *Polarstern* from 26 January to 06 March 2009 in the Atlantic sector of the Southern Ocean. The closed core of a stable cyclonic eddy in the Antarctic Polar Frontal Zone (48°S, 15°W; Figure S1 in the supporting information) was selected for the experiment based in part on real-time Eulerian and Lagrangian altimetry analyses, which were continued throughout the experiment (Okubo-Weiss and Lyapunov exponent techniques [*d'Ovidio et al*., 2009; *Smetacek et al*., 2012, supplementary information]).

[7] Starting on 27 January 2009, 2 t of Fe (10 t of $FeSO_4 \times 7$ H_2O) were dissolved in SF_6-labeled seawater with HCl and spread across 300 km^2 in the putative center of the eddy in a spiral pattern around two drifting buoys used to mark the patch center (theoretically yielding 2 nM Fe). Another 2 t of Fe were applied after 18 days, but an instrument fault prevented more SF_6 injection. The fertilized patch was studied for 39 days, comparing in-patch measurements to control out-patch observations in unfertilized waters of the eddy.

[8] The patch drifted within the eddy and was tracked via the drifting buoys, SF_6 concentration, the photosynthetic quantum efficiency F_V/F_M of phytoplankton, and the concentration of chlorophyll *a*. Because the SF_6 outgassed within about 2 weeks, we had to rely mostly on the buoys, chlorophyll *a*, and F_V/F_M, which were elevated within the patch until the end of the experiment. A total of five buoys had to be deployed in succession because the first two became detached from the main part of the patch.

2.2. Macronutrients and F_V/F_M

[9] $NO_3^- + NO_2^-$, NH_4^+, PO_4^{3-}, and $Si(OH)_4$ were measured at sea on a Skalar autoanalyzer using standard procedures.

[10] Phytoplankton photosynthetic quantum efficiency (F_V/F_M) was measured continuously from the underway seawater supply using a Chelsea Technology Group fast repetition rate fluorometer and averaged over 2 min intervals. Due to strong daytime fluorescence quenching, only F_V/F_M measurements from 19:00 to 06:00 local time were used.

2.3. Net Community Production (NCP) and Patch Model

[11] The seawater O_2 concentration is governed by biological and physical factors, but that of the inert gas argon (Ar) is governed only by physical factors. The seawater O_2:Ar ratio thus reflects biological O_2 supersaturation, $\Delta O_2/Ar$ [*Craig and Hayward*, 1987].

[12] O_2:Ar ratio was measured continuously in surface seawater by mass spectrometry, calibrated against outside air every 2–4 h, and averaged every 2 min [*Cassar et al*., 2009]. $\Delta O_2/Ar$ was calculated following *Craig and Hayward* [1987] and the biological O_2 concentration, $[O_2]_{Bio}$, according to *Cassar et al*. [2011]. In-patch $[O_2]_{Bio}$ was corrected for dilution with unfertilized waters using the dilution rate from a Lagrangian model of the patch and a weighting function based on the ventilation history of the mixed layer (see supporting information).

[13] NCP was estimated using both a steady state [*Reuer et al*., 2007] and a non–steady state calculation [*Hamme et al*., 2012]. The latter accounts for changes in $[O_2]_{Bio}$ over time.

[14] The piston velocity *k* was calculated from wind speed and water temperature measured in the entire eddy [*Wanninkhof*, 1992] (see supporting information).

[15] Routine calibration and instrument problems caused gaps of <1 h to several days, and there are no data for most of the final week. Thus, NCP was only analyzed up until Day 30 ($\Delta O_2/Ar$ at the very end of LOHAFEX was roughly equal to Day 30 values). Because of the gaps, the mean of the observations might not reflect the true mean NCP over the period; hence, loess models were fit to the in-patch data (see supporting information). NCP was then imputed from the models at 2 min frequency across all gaps. Mean NCP was calculated as the overall mean of measured and imputed NCP data up until Day 30 and converted to carbon as $C = O_2/1.4$ [*Laws*, 1991].

[16] Postcruise, the extent, trajectory, and dilution of the patch were modeled hourly using a filament-resolving Lagrangian model based on satellite altimetry data, F_V/F_M measurements, and surface buoy positions [*d'Ovidio et al*., 2010] (Figures S1a–S1f). Each O_2:Ar measurement was classed as in-patch, out-patch, or out-of-eddy based on this model, and the classification adjusted manually by comparison to F_V/F_M, chlorophyll, salinity, and ship location. The model agreed well with a satellite chlorophyll *a* image (Figure S2).

2.4. ^{234}Th Measurements

[17] Total ^{234}Th was measured in 4-L samples after manganese co-precipitation with a ^{230}Th yield monitor [*Cai et al*.,

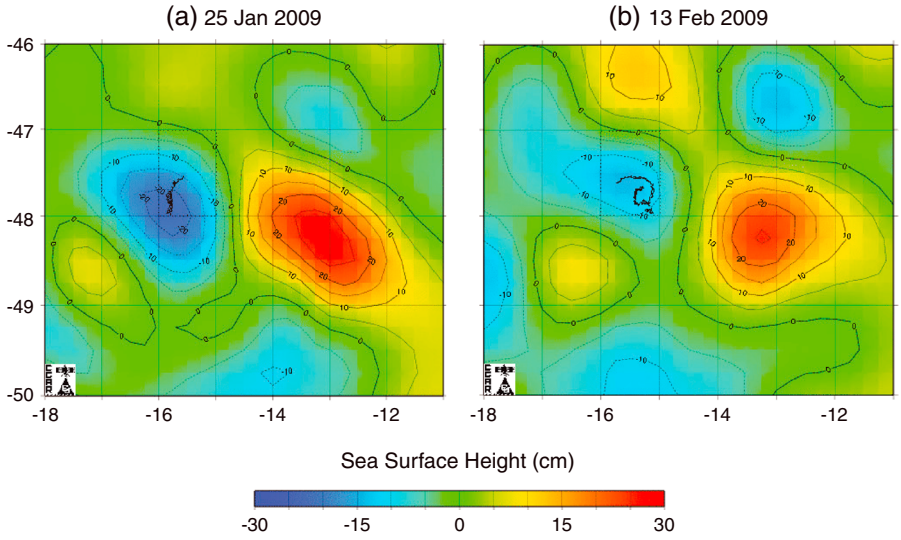

Figure 1. Satellite altimetry of the cyclonic eddy, in blue, in which a patch was fertilized. The solid black line shows the buoy (and thus patch) trajectories from (a) Days 0 to 5 and (b) Days 5 to 17. The eddy was entrained by the neighboring anticyclone (in red) toward the end of the experiment.

2006; *Pike et al*., 2005]. Since ^{234}Th deficits did not change over time, steady state downward ^{234}Th flux was calculated [*Coale and Bruland*, 1985, 1987]. In situ pumps (ISPs) with sequentially mounted 53 and 10 µm Nitex mesh collected particles at 10 stations from 100 m to measure POC:^{234}Th ratio. Particles were washed off the mesh with filtered seawater and sonication and filtered onto precombusted Whatman QMA filters, dried, and β counted. Following background β counting

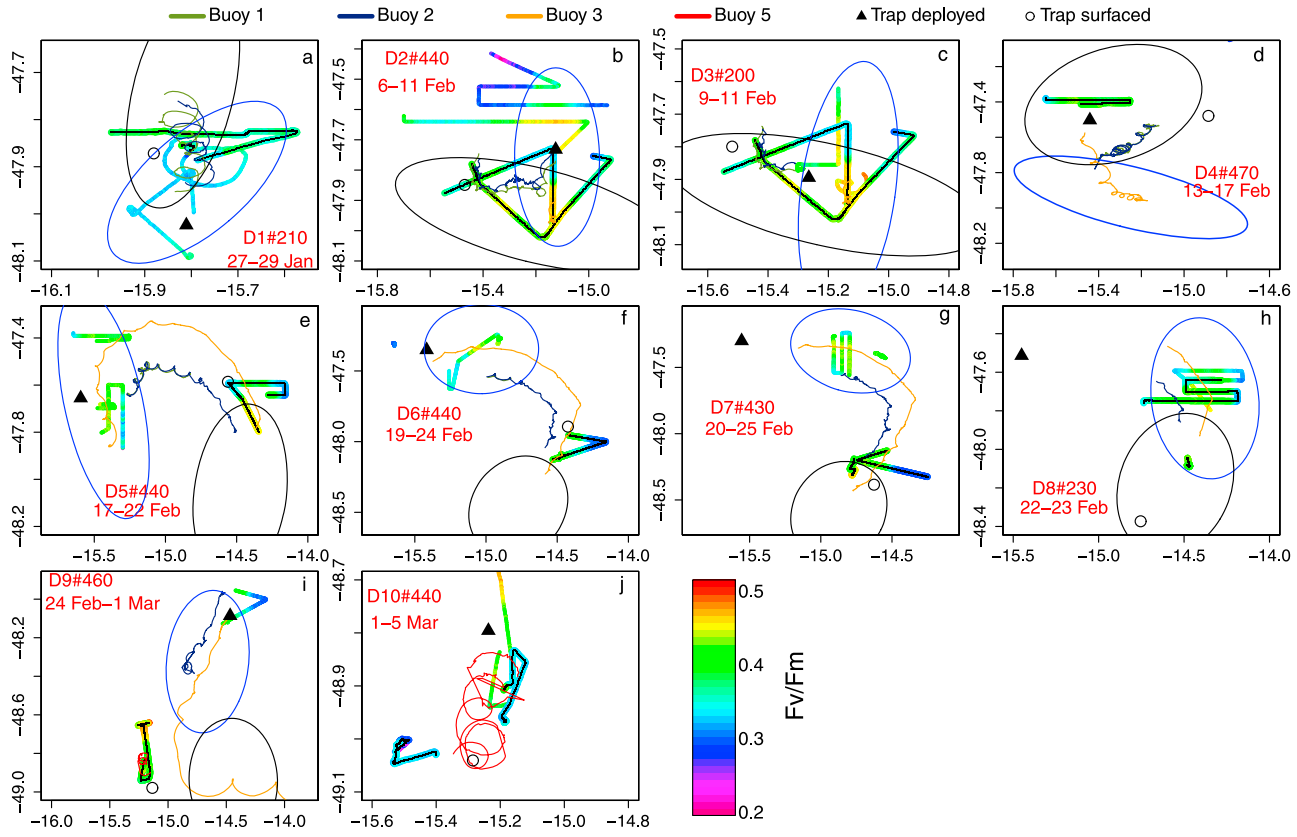

Figure 2. Maps of trap and drifting buoy trajectories, modeled patch positions, and nighttime underway F_V/F_M values along the ship's track. Blue ellipses show the patch positions when traps started collecting; black ellipses show the patch positions when traps stopped collecting. Only F_V/F_M values taken on the start and end days of collection are shown; measurements taken on the end day are marked with a small black dot at the center (this appears as a thin black line due to the high measurement frequency).

Table 1. Summary of Sediment Trap Collections[a]

Trap	In/Out	Collection Period	Dry Weight	POC	PON	POC:PON	Phyto POC (%)	Flagellate POC(%)	Opal	$CaCO_3$	^{234}Th
D1#210	In	27 Jan 21:30 to 29 Jan 21:25	55	0.46	0.053	8.7	8.7	8.1	0.085	0.12	63
D2#440	Probably In	06 Feb 15:00 to 11 Feb 14:00	81	0.70	0.082	8.5	1.4	1.1	0.16	0.19	NM
D3#200	Probably In	09 Feb 15:30 to 11 Feb 15:30	35	0.40	0.041	9.6	6.9	6.5	0.020	0.086	61
D4#470	Out	13 Feb 10:00 to 17 Feb 13:00	28	0.24[b]	0.027	8.7	9.1	8.0	0.060	0.14	NM
D5#440	In	17 Feb 13:00 to 22 Feb 16:00	110	0.77	0.089	8.6	1.9	1.7	0.16	0.29	NM
D6#440	In	19 Feb 10:15 to24 Feb 16:15	310	1.9[b]	0.22	8.6	5.0	4.6	0.30	0.49	690
D7#430	Out	20 Feb 04:00 to 25 Feb 16:00	99	0.91	0.11	8.4	2.1	1.7	0.11	0.27	510
D8#230	Out	22 Feb 16:15 to 23 Feb 06:15	140	2.4	0.25	9.4	0.30	0.24	0.10	0.47	780
D9#460	In	24 Feb 16:15 to 01 Mar 16:15	130	1.1	0.12	8.9	2.1	1.9	0.10	0.29	520
D10#440	In	01 Mar 17:00 to 05 Mar 07:00	100	1.1	0.12	8.9	4.1	3.7	0.082	0.32	NM

[a]Traps are referred to as Deployment Number # Depth. All fluxes are given in millimoles per square meter per day, rounded to two significant figures, except for ^{234}Th, which is in disintegrations per minute per square meter per day; the POC:PON ratios are in mol mol^{-1}. "NM" = not measured.
[b]These values are questionable; see section 3.5.

after ^{234}Th decay, filters were acidified with 0.1 *M* HCl, oven dried, and C and N measured on a Eurovector C/N element analyzer. POC:^{234}Th ratios were also measured in six sediment traps.

[18] Particulate (≥1 µm, QMA filter) and dissolved ^{234}Th were automatically sampled at 4 h resolution from the underway supply [*Rutgers van der Loeff et al.*, 2004, 2006]. Any automated measurements taken outside of the eddy were omitted, and the rest were designated as in- or out-patch measurements based on the patch model up to Day 31. Later measurements were designated "In" if they were within 10 nautical miles of the buoy. ^{234}Th data are presented as the activity ratio to ^{238}U ($^{238}U = 0.0713 \times \text{salinity} \pm 3\%$), which is 1 at secular equilibrium. The activity ratio for particulate ^{234}Th is to total ^{238}U in the water sample.

[19] Since In- and Out-patch ^{234}Th measurements did not differ, they were not affected by dilution.

2.5. Sediment Traps

[20] Neutrally buoyant PELAGRA traps [*Lampitt et al.*, 2008b] were deployed inside and outside of the patch at 200 and 450 m for 5–6 days each (Figure S3). Argo float profiles from the region suggested that 450 m would be close to, but still below, the winter mixed layer. Trap cups contained 2% borate-buffered formaldehyde in 0.2 µm filtered seawater with 0.5% wt/vol NaCl. Additional cups contained polyacrylamide gels [*Ebersbach and Trull*, 2008].

2.6. Sediment Trap Sample Analyses

[21] Samples from each trap were pooled, divided with a rotary splitter, and swimmers removed at sea (60–120× magnification). Samples were filtered on precombusted, preweighed Whatman GF/F filters (mass + POC + particulate organic nitrogen (PON)), polycarbonate filters (0.4 µm, particulate inorganic carbon (PIC) and biogenic silica (BSi)), or QMA filters (POC:^{234}Th ratios) and rinsed once with MilliQ. Blanks were prepared by filtering preservative through the different filters. POC:^{234}Th ratio was measured as for ISP samples; the other filters were stored at −20°C. Splits for phytoplankton cell counts and fecal pellet analysis were stored at +4°C.

[22] Dry weight, POC, PON, PIC, and BSi were measured as in *Martin et al.* [2011]. PIC samples were size fractionated [*Bairbakhish et al.*, 1999], but since the small fraction contained foram fragments, not coccoliths, we present the sum of both fractions.

[23] Fecal pellets were removed manually from one split onto a precombusted Whatman GF/F filter, acid fumed, oven dried, and POC analyzed at the University of California Davis Stable Isotope Facility.

[24] Too little material was available to replicate analyses. However, sample processing and analytical errors of 10–15% are likely for POC, PON, PIC, and BSi [*Martin*, 2011].

[25] Polyacrylamide gels were photographed on board following *Ebersbach and Trull* [2008]. Aliquots of each sample were settled in sedimentation chambers for 48 h and

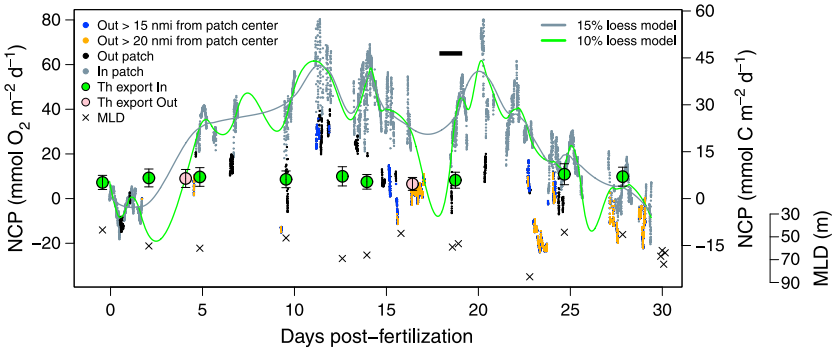

Figure 3. In- and out-patch NCP time series with ^{234}Th-derived export fluxes for comparison. Out-patch NCP measurements are color-coded by distance to the modeled patch center. The colored lines show two of the three loess models that were fit to the data. The solid black bar at 18 days shows when the patch was refertilized. Crosses indicate the mixed layer depth; the overall mean mixed layer depth was 66 m.

Table 2. Mean In-Patch NCP From Days 0–30, Corrected for Dilution With Unfertilized Waters[a]

Span of Loess Model	Mean NCP Steady State (mmol C m^{-2} d^{-1})	Mean NCP Non–Steady State (mmol C m^{-2} d^{-1})
10% of data	17	19
15% of data	21	22
20% of data	21	23

[a]Loess models spanning different percentages of the data were used to impute data across gaps; NCP values quoted are the mean of the measured and imputed data.

unicellular organisms counted under inverted light and epifluorescence microscopy. Mean biovolume was measured from 10 to 20 specimens per taxon [*Hillebrand et al*., 1999] and converted to organic carbon [*Menden-Deuer and Lessard*, 2000] to calculate unicellular plankton POC flux.

2.7. Underwater Video Profiler (UVP)

[26] The UVP is a rosette-mounted camera that photographs particles at ~0.2 m vertical resolution on the conductivity-temperature-depth downcast [*Picheral et al*., 2010]. Custom software calculates equivalent spherical diameter (ESD) and volume of all particles ≥100 μm and classes particles ≥ 630 μm ESD as either aggregates, fecal sticks/pellets, or live zooplankton [*Gorsky et al*., 2010] (Figure S10). Data were averaged over 5–10 min intervals for each individual profile. We present the median values of all in- and out-patch profiles here.

3. Results

3.1. Surface Biological and Biogeochemical Response to Fertilization

[27] Upon fertilization, F_V/F_M increased from ~0.33 and remained elevated at 0.4–0.5. In-patch chlorophyll *a* approximately doubled to 1–1.5 mg m^{-3}. Primary productivity from ^{14}C incubations was <80 mmol C m^{-2} d^{-1} outside, but rose up to a peak of 130 mmol C m^{-2} d^{-1} in the patch (M. Gauns, personal communication, 2010). In-patch NO_3^- declined from 20 to 17.5 μmol L^{-1}. $Si(OH)_4$ in the patch was 0.6–1.6 μmol L^{-1} and did not decrease over time.

[28] Diatoms were present but small for their species, and flagellates <10 μm contributed >90% of phytoplankton biomass (I. Schulz et al., in preparation, 2013). The coccolithophore *Emiliania huxleyi* declined after fertilization. Copepod grazing pressure was very high: fecal pellet production rates of *Calanus simillimus* implied grazing of >30% of net primary productivity (range: 0.7%–240%) (H. González et al., in preparation, 2013). *Oithona* spp. were particularly abundant: on average, 100,000 m^{-2} between 0 and 200 m in the patch (range: 35,000–235,000) (M. G. Mazzocchi, personal communication, 2010). Bacterial leucine and thymidine uptake increased somewhat upon fertilization, but cell abundance and species composition did not change [*Thiele et al*., 2012].

3.2. Movement of the Patch and Trap Trajectories

[29] The patch rotated inside the eddy core until Day 32 (27 February 2009, Figures S1a–S1f) and was then filamented when the fertilized eddy was entrained by a nearby anticyclone centered around 48°S, 13°W (Figure 1). The patch model (see section 2.3) indicated that the hot spot of the fertilized patch maintained its integrity until the end of the experiment, albeit shrinking due to erosion of its borders by stretching along the frontal jet. The patch model estimated an upper bound of dilution of the hot spot to 50% by Day 20 and to 20% by Day 39, mostly due to diffusion (Figure S4).

[30] The trap trajectories mirrored the surface circulation indicated by the buoys and shipboard acoustic Doppler current profiler (Figures 2 and S5), implying homogeneous circulation down to 450 m. Although D7#430 and D8#230 surfaced within the patch model, they were in fact recovered from waters outside of the patch. During this time, the patch was squeezed up against the eastern side of the eddy, with a very sharp boundary to unfertilized waters. Traps were designated as in or out (Table 1), yet none is truly unambiguous. Tracking the drift and boundaries of the patch was very challenging, and we cannot be sure that the In traps only collected below the patch. Conversely, time constraints limited how far away the out traps could be deployed, so they might have been influenced by the patch.

3.3. Net Community Production

[31] Steady state in-patch NCP rose from about 0 to 50 mmol O_2 m^{-2} d^{-1} by Day 10 and returned to zero by Day 30 (Figures 3 and S6). Out-patch NCP was consistently lower than in-patch NCP, and the out-patch data least likely to have been influenced by the patch (orange points in Figure 3) remained close to zero throughout the experiment. The nominally out-patch data on Days 10–14 were mostly very close to the patch, which were collected while steaming back and forth across the patch boundaries as we tried to map its extent, so their elevated NCP is likely due to mixing with fertilized waters. The autocorrelation function of $[O_2]_{Bio}$ indicated a strong diurnal cycle (Figure S7). The non–steady state estimate yielded higher NCP for the first half and lower NCP for the second half of the experiment (Figure S8). These differences cancelled each other out such that the overall mean NCP up to Day 30 was very similar to the steady state NCP (Table 2). We only discuss the steady state estimate below.

[32] A loess model spanning 15% of points was judged to fit the data best. Using fewer points yielded unlikely interpolations across gaps (green line in Figure 3), while using a higher percentage of points did not change the estimate significantly (Table 2).

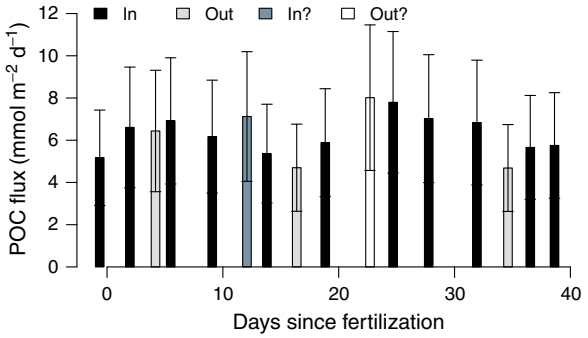

Figure 4. Export flux of POC calculated with a steady state model from the surface ^{234}Th deficit using a POC:^{234}Th ratio of 4.6 ± 2.0 μmol dpm^{-1}.

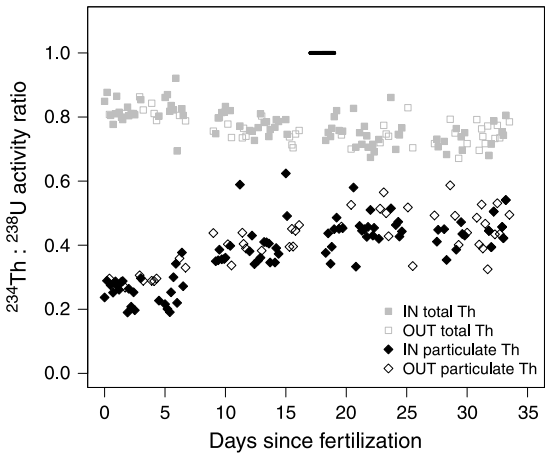

Figure 5. Activity ratios of ^{234}Th:^{238}U measured by the automated sampler from the underway supply. An activity ratio of 1 means that there is no depletion of ^{234}Th, and ratios <1 indicate depletion of ^{234}Th relative to ^{238}U. Activity ratios are shown both for particulate ^{234}Th and for total ^{234}Th (dissolved + particulate). The horizontal black bar at 18 days indicates the time of second fertilization.

[33] Our best estimate of mean in-patch NCP is thus 29 mmol O_2 m^{-2} d^{-1}, or 21 mmol C m^{-2} d^{-1} (Table 2), while out-patch NCP was −6.2 mmol O_2 m^{-2} d^{-1}, or −4.4 mmol C m^{-2} d^{-1}. The dilution correction only had a modest effect: uncorrected in-patch NCP was 25 mmol O_2 m^{-2} d^{-1}, or 18 mmol C m^{-2} d^{-1}. This is because mixed layer ventilation was ~sixfold faster than horizontal dilution, so most of the O_2 produced in the patch was lost to the atmosphere, not by dilution.

[34] Quantifying the uncertainty in NCP is unfortunately rather difficult. Estimating the piston velocity at high wind speeds is a major source of uncertainty [*Ho et al*., 2006]. However, O_2:Ar measurements seem to reflect NCP quite accurately in the Southern Ocean, though they may underestimate NCP by around 20% when productivity is high and Z_{mix} >50 m [*Jonsson et al*., 2013]. We therefore assume an uncertainty of at least ±20%, since the dilution correction and loess interpolation introduce additional uncertainties.

3.4. Export Based on ^{234}Th

[35] We calculated downward ^{234}Th flux assuming steady state, since the deficit did not change over time (Figure S9). ^{234}Th-derived export at 100 m was 5.2–7.8 mmol POC m^{-2} d^{-1} inside and 4.7–6.4 mmol m^{-2} d^{-1} outside of the patch (Figure 4). Most of the deficit was above 75 m, and ^{234}Th excesses relative to ^{238}U rarely exceeded the analytical error (Figure S9). The average ^{234}Th-derived in-patch export at 100 m was 6.3 mmol POC m^{-2} d^{-1}.

[36] There was no evidence of a fertilization-induced export event: export flux during Days 0–6 varied as much as during the entire experiment. Since it is bloom collapse that would trigger enhanced particle export [*Buesseler et al*., 1992, 2001; *Cochran et al*., 2000; *Martin et al*., 2011; *Smetacek et al*., 2012], the range in ^{234}Th-based export estimates over the first 6 days probably reflects spatial variability in the patch, not an increase upon fertilization.

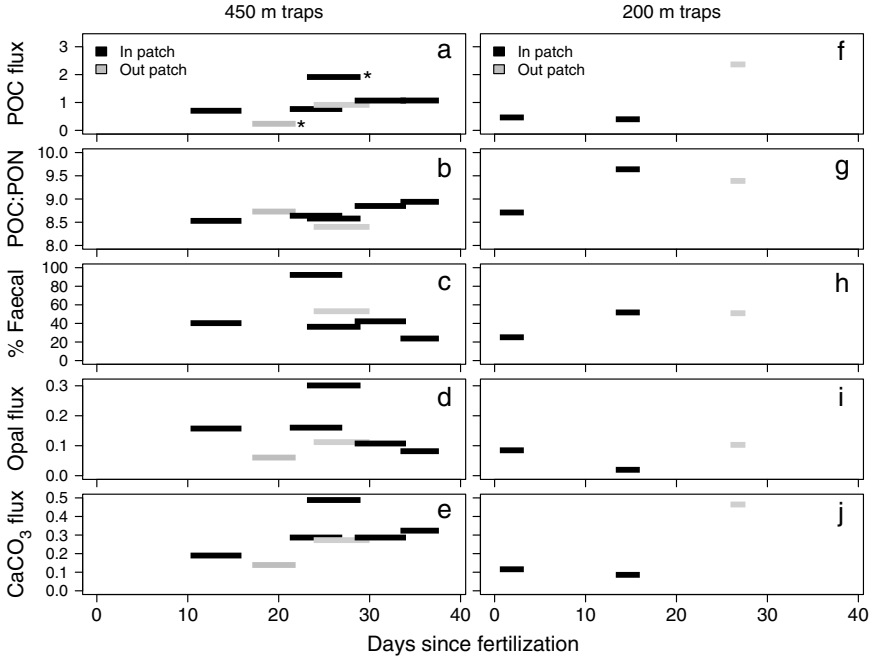

Figure 6. Fluxes intercepted by PELAGRA sediment traps. Each horizontal line represents one trap, with the line's length indicating the collection period. (a–e) Results from 450 m traps. (f–j) Results from 200 m traps. Note that the very low POC flux measured in trap D4#470 is probably erroneous, while the samples in trap D6#440 were compromised because the trap could not be recovered until 48 h after surfacing (see section 3). These data are marked with asterisks.

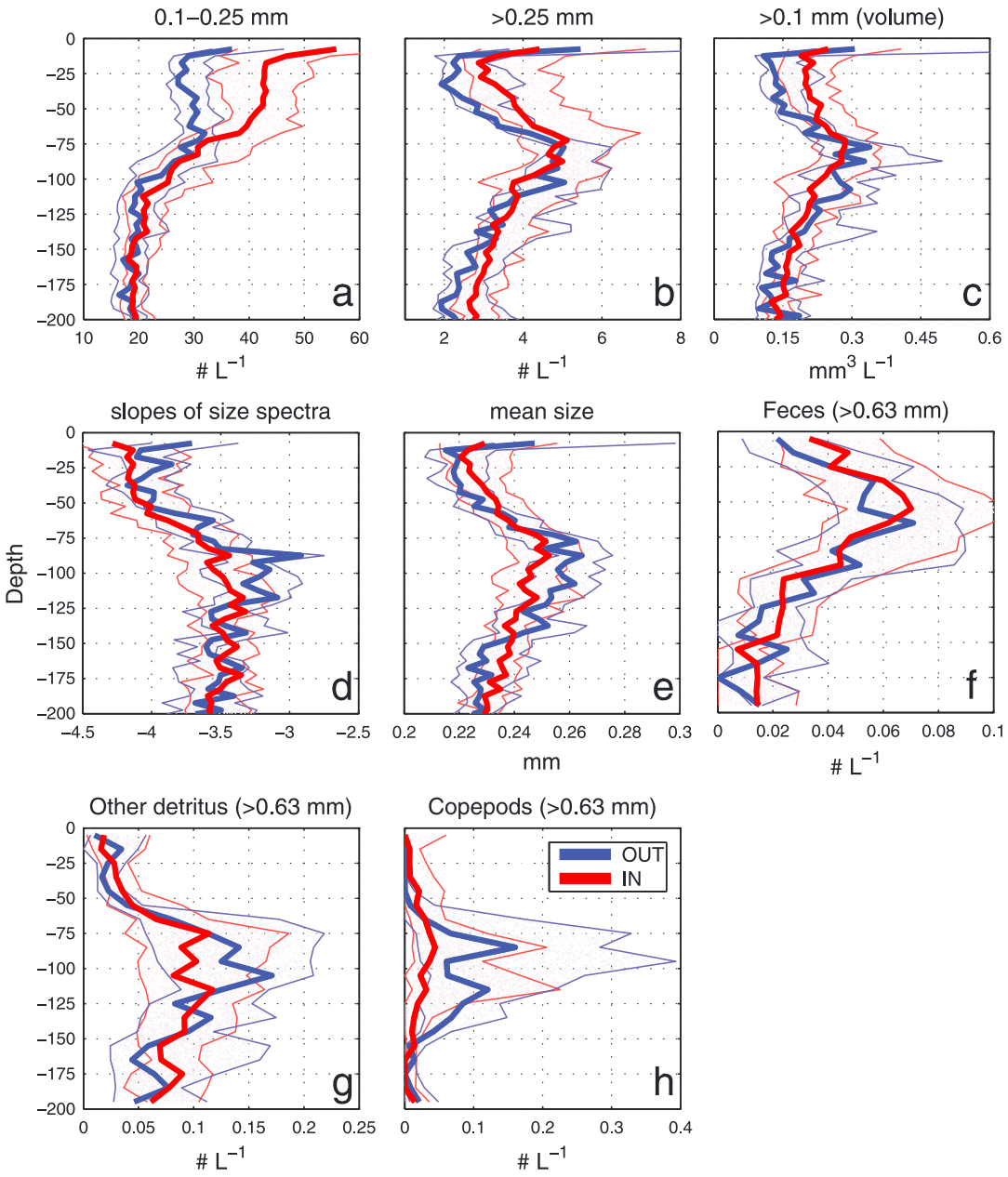

Figure 7. Data from the UVP, which detects any particles >100 µm ESD. (a, b) Median abundance of particles in two different size classes. (c) Volume concentration of all particles. (d) Slope of the size spectrum of particles. (e) Mean size of particles. (f–h) Abundances of fecal particles, unrecognizable detrital particles, and total copepods. Shaded areas show the interquartile range.

[37] POC:^{234}Th ratios were 2.9–6.9 µmol dpm^{-1} in the >53 µm ISP samples and 2.1–8.2 µmol dpm^{-1} in the three 200 m traps; the overall mean was 4.6 ± 2.0 µmol dpm^{-1}. In- and out-patch ratios fell within the same range, so one ratio was used for all stations. However, >53 µm Nitex-filtered particle samples are not necessarily representative of sinking particles (e.g., fragile particles may disintegrate and pass through the mesh). Hence, we also calculated the combined POC:^{234}Th ratio of all particles >10 µm from the ISP samples, which was 3.1 ± 0.7 µmol dpm^{-1}. Our ^{234}Th-derived POC export may thus be overestimated by about 30%, in which case export would actually have been in the range of 3.5–5.3 mmol POC m^{-2} d^{-1}.

[38] The automated surface measurements did not indicate a large export event either, and in- and out-patch surface ^{234}Th depletions were equal (Figure 5). While the total activity ratio of ^{234}Th:^{238}U declined from 0.8 initially to 0.75 by Day 39, ranging ±0.1 at any time, this does not indicate increased ^{234}Th depletion to 100 m depth. However, the particulate ^{234}Th fraction nearly doubled by Day 20. This evident increase in the surface area available for ^{234}Th scavenging could reflect either buildup of new or fragmentation of existing particles.

3.5. Trap Samples

[39] The traps recorded very low particle flux, and in-patch versus out-patch differences were not evident (Figure 6 and

Table 1). POC flux at 450 m was 0.70–1.9 mmol m^{-2} d^{-1} inside and 0.24–0.91 mmol m^{-2} d^{-1} outside of the patch. However, the lowest out-patch value (trap D4#470) was probably due to a sample processing error, while the highest in-patch value was from a trap that surfaced during adverse weather and could be recovered only 48 h later (trap D6#440); both values are hence suspect. At 200 m, POC flux was 0.46 mmol m^{-2} d^{-1} inside the patch (Days 0–2), but 2.4 mmol m^{-2} d^{-1} in one sample outside of the patch. POC:PON ratios were high: 8.4–9.6. Intact fecal pellets contributed around 45% of total POC flux (probably underestimated, as trap recovery and sample splitting might disintegrate pellets). The polyacrylamide gels were also dominated by fecal pellets. Unicellular plankton contributed only 0.3%–9% of total POC flux, mostly as dinoflagellates and other flagellates (Table 1). Broken and empty diatom frustules far outnumbered intact diatom cells.

[40] $CaCO_3$ flux exceeded opal flux by a factor of 2–7. Si:POC ratios were hence low (0.04–0.25), while moderate PIC:POC ratios were found (0.20–0.59).

[41] Strangely, ^{234}Th flux into the first and third traps was only 60 dpm m^{-2} d^{-1}, far lower than the >1000 dpm m^{-2} d^{-1} predicted at 100 m from ^{234}Th profiles. The other traps collected 510–780 dpm m^{-2} d^{-1}.

3.6. UVP Particle Profiles

[42] Particles <250 μm ESD were most abundant in the mixed layer, decreasing between 70 and 120 m. Particles >250 μm ESD peaked at 75 m, decreasing down to 150 m (Figure 7). Total particle volume peaked at 75 m and decreased to about 150 m; while mean particle size and the slope of the particle size spectrum both indicate a higher proportion of large particles below the mixed layer. Moreover, while fecal abundance peaked at 50 m and then decreased sharply to 150 m, unrecognizable detritus (that would include fecal pellets disintegrated by coprorhexy) [*Lampitt et al*., 1990] increased sharply from 50 to 80 m (Figures 7 and S10). Total copepod abundance peaked at 75–100 m.

[43] Since particles in the 250–630 μm and >630 μm size classes had very similar depth profiles, the two classes are combined in Figure 7. However, particles <630 μm ESD were more abundant inside than outside the patch (Mann-Whitney U test, $W = 196$, $n = 26$, and 9, $p = 0.02$), and the mean abundance and volume of particles >630 μm ESD decreased with time in 100 m below the mixed layer inside the patch (Spearman's rho = −0.55, $n = 26$, $p = 0.004$). No other significant trends with time or in-patch versus out-patch differences were found (for time series of abundance and volume, see Figure S11).

4. Discussion

4.1. Effect of Fertilization on Downward Particle Flux

[44] Neither the ^{234}Th nor the sediment trap data indicate major fertilization-induced export, despite the clear increase in NCP. Moreover, the UVP showed no increase in particles >100 μm upon fertilization. In contrast, evidence is mounting that iron fertilization of Si-replete waters, leading to diatom blooms, can induce severalfold higher export than during LOHAFEX and enhance flux to deep waters (EIFEX [*Smetacek et al*., 2012], CROZEX [*Salter et al*., 2007; *Morris and Sanders*, 2012], SEEDS II [*Aramaki et al*., 2009], SERIES [*Boyd et al*., 2005], SOFeX [*Buesseler et al*., 2004], KEOPS [*Blain et al*., 2007], and IronEx-II [*Bidigare et al*., 1999]).

[45] The LOHAFEX data thus suggest that iron fertilization of Si-limited Southern Ocean waters, which does not stimulate diatom blooms, enhances neither shallow export nor deep POC flux. This is consistent with the view that diatoms are major contributors to new production [*Dugdale and Wilkerson*, 1998, 2001], given the importance that sinking may have in diatom ecology [*Smetacek*, 1985; *Salter et al*., 2012]. It has hence been questioned whether Southern Ocean iron fertilization would work at all to enhance carbon sequestration if it does not do so under Si limitation, because Si is already fully utilized in the Southern Ocean [*Trull et al*., 2001b]. However, iron fertilization can lower the Si:C ratio of exported material and, thus, can sequester more carbon for the same amount of Si [*Smetacek et al*., 2012; see also *Salter et al*., 2012]. Thus, we do not believe that the LOHAFEX results imply that iron fertilization cannot enhance Southern Ocean carbon sequestration.

[46] However, we cannot readily disentangle the effects on downward POC flux of the lack of diatoms on the one hand and the very high grazing pressure and particle reprocessing by zooplankton on the other. Thus, LOHAFEX provides no conclusive proof that downward POC flux in low-Si sub-Antarctic waters will never be enhanced by iron fertilization, especially since significant export and deep POC flux do occur in low-Si regions [*Cardinal et al*., 2005; *Henson et al*., 2012; *Honjo et al*., 2008; *Planchon et al*., 2013; *Trull et al*., 2001a]. Organic carbon did accumulate in the mixed layer (section 4.2), leaving open the possibility that enhanced export occurred after the end of the experiment, although the heavy grazing and particle reprocessing by zooplankton would probably have strongly attenuated any future export event.

[47] Nevertheless, our results agree with those of SAZ-SENSE, which reported lower export and greater mesopelagic remineralization in naturally iron-replete than in iron-limited low-Si sub-Antarctic waters [*Bowie et al*., 2011; *Ebersbach et al*., 2011; *Jacquet et al*., 2011]. Only a modest response, mostly by nondiatom phytoplankton <20 μm, was found upon iron fertilization of sub-Antarctic low-Si waters during SAGE, suggesting that export was probably not greatly enhanced [*Harvey et al*., 2010; *Peloquin et al*., 2010]. In contrast, POC export at the low-Si sub-Antarctic SOFeX North site was enhanced by iron fertilization, with NO_3^- depletion similar to LOHAFEX [*Bishop et al*., 2004; *Coale et al*., 2004]. However, $Si(OH)_4$ in SOFeX North was above limiting concentrations and, apparently, replenished in the elongated patch by admixture of surrounding water. Weakly silicified diatoms contributed 44% to total phytoplankton POC and aggregated eventually [*Coale et al*., 2004]. Thus, while SOFeX North is nominally considered a "low-Si" experiment, diatoms were not initially Si limited and did bloom, in strong contrast to LOHAFEX.

4.2. Comparison Between NCP, ^{234}Th, and Sediment Traps

[48] Comparing these three methods is fraught with complications, since export may lag production, the methods integrate over different time scales and depths, and each suffers from biases and uncertainties [*Lampitt et al*., 2008b;

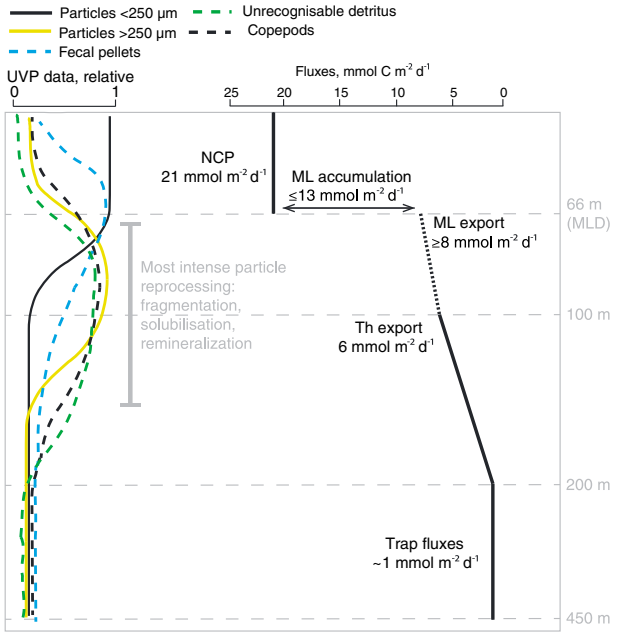

Figure 8. Overview of carbon fluxes and particle profiles during LOHAFEX. The right side summarizes the carbon fluxes: NCP averaged 21 mmol m^{-2} d^{-1} in the mixed layer, of which ≤13 mmol m^{-2} d^{-1} accumulated in the mixed layer, leaving at least 8 mmol m^{-2} d^{-1} for export below the mixed layer. The dotted line indicates that mixed layer export is not very well constrained, and thus, the degree of flux attenuation between the mixed layer and 100 m is uncertain. ^{234}Th-derived export exceed the flux caught in sediment traps, indicating further attenuation from 100 to 200 m. The left side of the figure summarizes the UVP data, with abundance of different particle types indicated on a relative axis. The UVP data collectively indicate that particle transformation was most intense between the base of the mixed layer and 150 m, most likely owing to zooplankton activity; flux attenuation was most likely intense throughout this range.

Le Moigne et al., 2013; *Morris et al.*, 2007; *Savoye et al.*, 2008]. However, the long duration and Lagrangian nature of LOHAFEX mitigate some of these problems, and while significant uncertainties are associated with each of our estimates, we do not believe that any of the methods is grossly biased. Figure 8 summarizes our main conclusions.

[49] NCP was 21 mmol POC m^{-2} d^{-1}, exceeding the 100 m export flux by ~15 mmol m^{-2} d^{-1}, implying organic carbon accumulation in the mixed layer and/or flux attenuation between the mixed layer depth (MLD) and 100 m. Direct measurements do suggest accumulation in the mixed layer of ≤6 µmol L^{-1} of total organic carbon in the patch (S. W. A. Naqvi et al., in preparation, 2013), accounting for ≤13 mmol m^{-2} d^{-1} of the NCP. This would allow for export out of the mixed layer of at least 8 mmol POC m^{-2} d^{-1}, of which around 6 mmol m^{-2} d^{-1} sank below 100 m (as diagnosed from ^{234}Th). This implies that POC flux was attenuated by around 2 mmol m^{-2} d^{-1} between the mixed layer and 100 m. Thus, a little more than half of the in-patch NCP appears to have accumulated in the mixed layer, while the remainder was exported below the mixed layer as sinking POC flux.

[50] The POC flux diagnosed from ^{234}Th exceeded trap fluxes threefold to sixfold. Since the flux of ^{234}Th itself was just 2–3 times lower in the traps than that diagnosed from the profiles, the discrepancy cannot be attributed purely to biased trap collection. The ^{234}Th and trap data thus indicate a strong reduction in particle flux from 100 to 200–450 m.

[51] Between the base of the mixed layer and the sediment traps at 200–450 m, POC flux was probably attenuated about eightfold, or about sixfold between 100 and 200–450 m. These estimates must be treated with caution, since the export estimates at each depth carry significant uncertainty. However, such intense attenuation contrasts with the higher transfer efficiencies of flux to depth that have been reported upon collapse of diatom blooms [*Buesseler and Boyd*, 2009; *Martin et al.*, 2011; *Smetacek et al.*, 2012]. Interestingly, subsurface ^{234}Th excesses indicative of remineralization [*Maiti et al.*, 2010; *Savoye et al.*, 2004] were not consistently found, although excesses are often confined to narrow depth horizons. They might hence have been missed by our 50 m vertical resolution in the mesopelagic.

[52] The UVP data are also consistent with strong flux attenuation: particle stocks declined with depth below the MLD, and there was a shift from intact fecal pellets to unrecognizable detritus. This shift was most pronounced at the depth of highest copepod abundance, implying coprorhexy [*Lampitt et al.*, 1990] and, generally, particle reprocessing by zooplankton. The high abundance of *Oithona* spp. during LOHAFEX also suggests substantial flux reprocessing: *Oithona* spp. are reported to be coprophagous and, hence, likely to attenuate POC flux [*González and Smetacek*, 1994]. However, intact fecal material contributed ~45% to the sediment trap catches, underscoring the importance of unreprocessed fecal pellets in downward POC flux.

[53] This contrasts with the enhanced mesopelagic particle stocks seen during the Kerguelen Ocean and Plateau Compared Study (KEOPS) [*Jouandet et al.*, 2011]. Overall, the UVP revealed that the most intense particle transformations took place between the base of the mixed layer and around 150 m (Figures 7 and S8), and flux attenuation probably took place throughout this depth range.

[54] Mesopelagic communities of high- and low-Si regions may actually respond differently to iron fertilization: mesopelagic remineralization as estimated from excess barium was a relatively low proportion of export flux in the high-Si iron fertilized areas of EIFEX and KEOPS [*Jacquet et al.*, 2008a, 2008b]. In contrast, at the iron-replete low-Si sub-Antarctic site in SAZ-SENSE a greater proportion of export flux was remineralized than at either of the iron-limited sites [*Jacquet et al.*, 2011]. Moreover, export from SOFeX North was initially reduced owing to a response by mesopelagic grazers, though an export event did occur later [*Bishop et al.*, 2004; *Lam and Bishop*, 2007]. We observed no drastic changes over time, but the upper mesopelagic community appeared to attenuate particle flux heavily.

5. Conclusions

[55] Downward particle flux out of the fertilized patch and through the mesopelagic was tracked successfully for 39 days. Net community production, but not 100 m export flux, increased relative to unfertilized waters; mixed layer organic carbon accumulation and flux attenuation above 100 m can

account for this difference. Particle flux appeared to decrease strongly between 100 and 200–450 m. Our results add further evidence to support the idea that Fe fertilization does not necessarily stimulate POC export and sequestration under Si limitation in the Southern Ocean. Zooplankton community composition and activity under the mixed layer may strongly regulate the export by reprocessing sinking particles and altering the particle size distribution.

[56] **Acknowledgments.** We thank the captain and crew of R/V *Polarstern*. Kevin Saw ensured the success of the PELAGRA deployments, Christine Klaas gave advice on the dilution correction, and two anonymous reviewers provided constructive criticism that significantly improved the manuscript. The altimeter products were produced by Ssalto/Duacs and distributed by AVISO with support from CNES. N.C. was partly supported by an Alfred P. Sloan Fellowship. This work formed part of the PhD research of P.M.

References

Aramaki, T., Y. Nojiri, and K. Imai (2009), Behaviour of particulate materials during iron fertilization experiments in the Western Subarctic Pacific (SEEDS and SEEDS II), *Deep Sea Res., Part II*, *56*, 2875–2888.

Aumont, O., and L. Bopp (2006), Globalizing results from ocean in situ iron fertilization studies, *Global Biogeochem. Cycles*, *20*, GB2017, doi:10.1029/2005GB002591.

Bairbakhish, A. N., J. Bollmann, C. Sprengel, and H. R. Thierstein (1999), Disintegration of aggregates and coccospheres in sediment trap samples, *Mar. Micropaleontol.*, *37*, 219–223.

Bidigare, R. R., et al. (1999), Iron-stimulated changes in ^{13}C fractionation and export by equatorial Pacific phytoplankton: Toward a paleogrowth rate proxy, *Paleoceanography*, *14*, 589–595.

Bishop, J. K. B., T. J. Wood, R. E. Davis, and J. T. Sherman (2004), Robotic observations of enhanced carbon biomass and export at 55°S during SOFeX, *Science*, *304*, 417–420, doi:10.1126/science.1087717.

Blain, S., et al. (2007), Effect of natural iron fertilization on carbon sequestration in the Southern Ocean, *Nature*, *446*, 1070–1074, doi:10.1038/nature05700.

Bowie, A. R., T. W. Trull, and F. Dehairs (2011), Estimating the sensitivity of the subantarctic zone to environmental change: The SAZ-Sense project, *Deep Sea Res., Part II*, *58*, 2051–2058, doi:10.1016/j.dsr2.2011.05.034.

Boyd, P. W., and T. W. Trull (2007), Understanding the export of biogenic particles in oceanic waters: Is there consensus?, *Prog. Oceanogr.*, *72*, 276–312, doi:10.1016/j.pocean.2006.10.007.

Boyd, P. W., et al. (2005), The evolution and termination of an iron-induced mesoscale bloom in the Northeast Subarctic Pacific, *Limnol. Oceanogr.*, *50*, 1872–1886.

Boyd, P. W., et al. (2007), Mesoscale iron enrichment experiments 1993–2005: Synthesis and future directions, *Science*, *315*, 612–617, doi:10.1126/science.1131669.

Buesseler, K. O., and P. W. Boyd (2009), Shedding light on processes that control particle export and flux attenuation in the twilight zone of the open ocean, *Limnol. Oceanogr.*, *54*, 1210–1232.

Buesseler, K. O., M. P. Bacon, J. K. Cochran, and H. D. Livingston (1992), Carbon and Nitrogen Export During the JGOFS North-Atlantic Bloom Experiment Estimated from Th-234:U-238 Disequilibria, *Deep Sea Res., Part A*, *39*, 1115–1137.

Buesseler, K. O., L. Ball, J. Andrews, J. K. Cochran, D. J. Hirschberg, M. P. Bacon, A. Fleer, and M. Brzezinski (2001), Upper ocean export of particulate organic carbon and biogenic silica in the Southern Ocean along 170ºW, *Deep Sea Res., Part II*, *48*, 4275–4297.

Buesseler, K. O., J. E. Andrews, S. M. Pike, and M. A. Charette (2004), The effects of iron fertilization on carbon sequestration in the Southern Ocean, *Science*, *304*, 414–417, doi:10.1126/science.1086895.

Cai, P., M. Dai, D. Lv, and W. Chen (2006), An improvement in the small-volume technique for determining thorium-234 in seawater, *Mar. Chem.*, *100*, 282–288.

Cardinal, D., N. Savoye, T. W. Trull, L. André, E. E. Kopczynska, and F. Dehairs (2005), Variations of carbon remineralisation in the Southern Ocean illustrated by the Ba_{xs} proxy, *Deep Sea Res., Part I*, *52*, 355–370.

Cassar, N., B. A. Barnett, M. L. Bender, J. Kaiser, R. C. Hamme, and B. Tilbrook (2009), Continuous high-frequency dissolved O_2/Ar measurements by equilibrator inlet mass spectrometry, *Anal. Chem.*, *81*, 1855–1864.

Cassar, N., P. J. D. DiFiore, B. A. Barnett, M. L. Bender, A. R. Bowie, B. Tilbrook, K. Petrou, K. J. Westwood, S. W. Wright, and D. Lefevre (2011), The influence of iron and light on net community production in the Subantarctic and Polar Frontal Zones, *Biogeosciences*, *8*, 227–237, doi:10.5194/bg-8-227-2011.

Coale, K. H., and K. W. Bruland (1985), ^{234}Th:^{238}U disequilibria within the California Current, *Limnol. Oceanogr.*, *30*, 22–33.

Coale, K. H., and K. W. Bruland (1987), Oceanic stratified euphotic zone as elucidated by ^{234}Th:^{238}U disequilibria, *Limnol. Oceanogr.*, *32*, 189–200.

Coale, K. H., et al. (2004), Southern Ocean iron enrichment experiment: Carbon cycling in high- and low-Si waters, *Science*, *304*, 408–414, doi:10.1126/science.1089778.

Cochran, J. K., K. O. Buesseler, M. P. Bacon, H. W. Wang, D. J. Hirschberg, L. Ball, J. Andrews, G. Crossin, and A. Fleer (2000), Short-lived thorium isotopes (^{234}Th, ^{228}Th) as indicators of POC export and particle cycling in the Ross Sea, Southern Ocean, *Deep Sea Res., Part II*, *47*, 3451–3490, doi:10.1016/S0967-0645(00)00075-8.

Craig, H., and T. Hayward (1987), Oxygen supersaturation in the ocean: Biological versus physical contributions, *Science*, *235*, 199–202.

de Baar, H. J. W., et al. (2005). Synthesis of iron fertilization experiments: from the Iron Age in the Age of Enlightenment, *J. Geophys. Res.*, *110*, C09S16, doi:10.1029/2004JC002601.

d'Ovidio, F., J. Isern-Fontanet, C. López, E. García-Ladona, and E. Hernández-García (2009), Comparison between Eulerian diagnostics and the finite-size Lyapunov exponent computed from altimetry in the Algerian Basin, *Deep Sea Res., Part I*, *56*, 15–31, doi:10.1016/j.dsr.2008.07.014.

d'Ovidio, F., S. De Monte, S. Alvain, Y. Dandonneau, and M. Lévy (2010), Fluid dynamical niches of phytoplankton types, *Proceedings of the National Academy of Sciences of the United States of America*, *107*, 18,366–18,370, doi:10.1073/pnas.1004620107.

Dugdale, R. C., and F. P. Wilkerson (1998), Silicate regulation of new production in the equatorial Pacific upwelling, *Nature*, *391*, 270–273.

Dugdale, R. C., and F. P. Wilkerson (2001), Sources and fates of silicon in the ocean: The role of diatoms in the climate and glacial cycles, *Sci. Mar.*, *65*, 141–152.

Ebersbach, F., and T. W. Trull (2008), Sinking particle properties from polyacrylamide gels during the KErguelen Ocean and Plateau compared Study (KEOPS): Zooplankton control of carbon export in an area of persistent natural iron inputs in the Southern Ocean, *Limnol. Oceanogr.*, *53*, 212–224.

Ebersbach, F., T. W. Trull, D. M. Daviel, and S. G. Bray (2011), Mesopelagic particle fluxes in the Sub-Antarctic and Polar Frontal Zones in the Southern Ocean south of Australia in summer—Perspectives from free-drifting sediment traps, *Deep Sea Res., Part II*, *58*, 2260–2276, doi:10.1016/j.dsr2.2011.05.025.

González, H. E., and V. Smetacek (1994), The possible role of the cyclopoid copepod *Oithona* in retarding vertical flux of zooplankton faecal material, *Mar. Ecol. Prog. Ser.*, *113*, 233–246.

Gorsky, G., M. D. Ohman, M. Picheral, S. Gasparini, L. Stemmann, J.-B. Romagnan, A. Cawood, S. Pesant, C. Garcia-Comas, and F. Prejger (2010), Digital zooplankton image analysis using the ZooScan integrated system, *J. Plankton Res.*, *32*, 285–303, doi:10.1093/plankt/fbp124.

Hamme, R. C., et al. (2012), Dissolved O_2/Ar and other methods reveal rapid changes in productivity during a Lagrangian experiment in the Southern Ocean, *J. Geophys. Res.*, *117*, C00F12, doi:10.1029/2011JC007046.

Harvey, M. J., et al. (2010), The SOLAS air-sea gas exchange experiment (SAGE) 2004, *Deep Sea Res., Part II*, *58*, 753–763, doi:10.1016/j.dsr2.2010.10.015.

Henson, S., R. Sanders, and E. Madsen, (2012), Global patterns of in efficiency of particulate organic carbon export and transfer to the deep ocean, *Global Biogeochem. Cycles*, *26*, GB1028, doi:10.1029/2011GB004099.

Hillebrand, H., C.-D. Dürselen, D. Kirschtel, U. Pollinger, and Z. Tamar (1999), Biovolume calculation for pelagic and benthic microalgae, *J. Phycol.*, *35*, 403–424.

Ho, D. T., C. S. Law, M. J. Smith, P. Schlosser, M. Harvey, and P. Hill (2006), Measurements of air-sea gas exchange at high wind speeds in the Southern Ocean: Implications for global parameterizations, *Geophys. Res. Lett.*, *33*, L16611, doi:10.1029/2006GL026817.

Honjo, S., S. J. Manganini, R. A. Krishfield, and R. Francois (2008), Particulate organic carbon fluxes to the ocean interior and factors controlling the biological pump: A synthesis of global sediment trap programs since 1983, *Prog. Oceanogr.*, *76*, 217–285, doi:10.1016/j.pocean.2007.11.003.

Jacquet, S. H. M., F. Dehairs, N. Savoye, I. Obernosterer, U. Christaki, C. Monnin, and D. Cardinal (2008a), Mesopelagic organic carbon remineralization in the Kerguelen Plateau region tracked by biogenic particulate Ba, *Deep Sea Res., Part II*, *55*, 868–879, doi:10.1016/j.dsr2.2007.12.038.

Jacquet, S. H. M., N. Savoye, F. Dehairs, V. H. Strass, and D. Cardinal (2008b), Mesopelagic carbon remineralization during the European Iron Fertilization Experiment, *Global Biogeochem. Cycles*, *22*, GB1023, doi:10.1029/2006GB002902.

Jacquet, S. H. M., F. Dehairs, I. Dumont, S. Becquevort, A.-J. Cavagna, and D. Cardinal (2011), Twilight zone organic carbon remineralization in the

Polar Front Zone and Subantarctic Zone south of Tasmania, *Deep Sea Res., Part II*, *58*, 2222–2234, doi:10.1016/j.dsr2.2011.05.029.

Jonsson, B. F., S. C. Doney, J. Dunne, and M. Bender (2013), Evaluation of Southern Ocean O_2/Ar-based NCP estimates in a model framework, *J. Geophys. Res.: Biogeosci.*, *118*, 385–399, doi:10.1002/jgrg.20032.

Jouandet, M.-P., T. W. Trull, L. Guidi, M. Picheral, F. Ebersbach, L. Stemmann, and S. Blain (2011), Optical imaging of mesopelagic particles indicates deep carbon flux beneath a natural iron-fertilized bloom in the Southern Ocean, *Limnol. Oceanogr.*, *56*, 1130–1140.

Kwon, E. Y., F. Primeau, and J. L. Sarmiento (2009), The impact of remineralization depth on the air-sea carbon balance, *Nat. Geosci.*, *2*, 630–635, doi:10.1038/ngeo612.

Lam, P. J., and J. K. B. Bishop (2007), High biomass, low export regimes in the Southern Ocean, *Deep Sea Res., Part II*, *54*, 601–638, doi:10.1016/j.dsr2.2007.01.013.

Lampitt, R. S., T. Noji, and B. von Bodungen (1990), What happens to zooplankton faecal pellets? Implications for material flux, *Mar. Biol.*, *104*, 15–23.

Lampitt, R. S., et al. (2008a), Ocean fertilization: A potential means of geoengineering?, *Philos. Trans. R. Soc. A.*, *366*, 3919–3945.

Lampitt, R. S., B. Boorman, L. Brown, M. Lucas, I. Salter, R. Sanders, K. Saw, S. Seeyave, S. J. Thomalla, and R. Turnewitsch (2008b), Particle export from the euphotic zone: Estimates using a novel drifting sediment trap, Th-234 and new production, *Deep Sea Res., Part I*, *55*, 1484–1502, doi:10.1016/j.dsr.2008.07.002.

Laws, E. A. (1991), Photosynthetic quotients, new production and net community production in the open sea, *Deep Sea Res.*, *38*, 143–167.

Le Moigne, F. A. C., M. Villa-Alfageme, R. J. Sanders, C. Marsay, S. Henson, and R. García-Tenorio (2013), Export of organic carbon and biominerals derived from ^{234}Th and ^{210}Po at the Porcupine Abyssal Plain, *Deep Sea Res., Part I*, *72*, 88–101, doi:10.1016/j.dsr.2012.10.010.

Lenton, T. M., and N. E. Vaughan (2009), The radiative forcing potential of different climate geoengineering options, *Atmos. Chem. Phys.*, *9*, 5539–5561.

Lomas, M. W., D. K. Steinberg, T. Dickey, C. A. Carlson, N. B. Nelson, R. H. Condon, and N. R. Bates (2010), Increased ocean carbon export in the Sargasso Sea linked to climate variability is countered by its enhanced mesopelagic attenuation, *Biogeosciences*, *7*, 57–70, doi:10.5194/bg-7-57-2010.

Maiti, K., C. R. Benitez-Nelson, and K. O. Buesseler (2010), Insights into particle formation and remineralization using the short-lived radionuclide, Thorium-234, *Geophys. Res. Lett.*, *37*, L15608, doi:10.1029/2010GL044063.

Martin, P. (2011), Particle Export and Flux Through the Mesopelagic in the High-Latitude North and South Atlantic, PhD thesis, Sch. of Ocean and Earth Sci., Univ. of Southampton, Southampton, U. K.

Martin, P., R. S. Lampitt, M. J. Perry, R. Sanders, C. Lee, and E. D'Asaro (2011), Export and mesopelagic particle flux during a North Atlantic spring bloom, *Deep Sea Res., Part I*, *58*, 338–349, doi:10.1016/j.dsr.2011.01.006.

Menden-Deuer, S., and E. J. Lessard (2000), Carbon to volume relationship for dinoflagellates, diatoms, and other protist plankton, *Limnol. Oceanogr.*, *45*, 569–579.

Morris, P. J., and R. Sanders (2012), A carbon budget for a naturally iron fertilized bloom in the Southern Ocean, *Global Biogeochem. Cycles*, *25*, GB3004, doi:10.1029/2010GB003780.

Morris, P. J., R. Sanders, R. Turnewitsch, and S. Thomalla (2007), ^{234}Th-derived particulate organic carbon export from an island-induced phytoplankton bloom in the Southern Ocean, *Deep Sea Res., Part II*, *54*, 2208–2232, doi:10.1016/j.dsr2.2007.06.002.

Parekh, P., S. Dutkiewicz, M. J. Follows, and T. Ito (2006), Atmospheric carbon dioxide in a less dusty world, *Geophys. Res. Lett.*, *33*, L03610, doi:10.1029/2005GL025098.

Peloquin, J., J. Hall, K. Safi, W. O. Smith, S. Wright, and R. Enden (2010), The response of phytoplankton to iron enrichment in sub-Antarctic HNLCLSi waters: Results from the SAGE experiment, *Deep Sea Res., Part II*, *58*, 808–823, doi:10.1016/j.dsr2.2010.10.021.

Picheral, M., L. Guidi, L. Stemmann, D. M. Karl, G. Iddaoud, and G. Gorsky (2010), The Underwater Vision Profiler 5: An advanced instrument for high spatial resolution studies of particle size spectra and zooplankton, *Limnol. Oceanogr. Methods*, *8*, 462–473.

Pike, S. M., K. O. Buesseler, J. Andrews, and N. Savoye (2005), Quantification of ^{234}Th recovery in small volume sea water samples by inductively coupled plasma-mass spectrometry, *J. Radioanal. Nucl. Chem.*, *263*, 355–360.

Planchon, F., A.-J. Cavagna, D. Cardinal, L. André, and F. Dehairs (2013), Late summer particulate organic carbon export and twilight zone remineralization in the Atlantic sector of the Southern Ocean, *Biogeosciences*, *10*, 803–820, doi:10.5194/bg-10-803-2013.

Pollard, R. T., et al. (2009), Southern Ocean deep-water carbon export enhanced by natural iron fertilization, *Nature*, *457*, 577–580, doi:10.1038/nature07716.

Reuer, M. J., B. A. Barnett, M. L. Bender, P. G. Falkowski, and M. B. Hendricks (2007), New estimates of Southern Ocean biological production rates from O_2/Ar ratios and the triple isotope composition of O_2, *Deep Sea Res., Part I*, *54*, 951–974, doi:10.1016/j.dsr.2007.02.007.

Rutgers van der Loeff, M., I. Vöge, and H. Lilienthal (2004), Automatisiertes filtrationsverfahren und filtrationssystem zur verfahrensdurchführung, Patent 102004040248, Germany.

Rutgers van der Loeff, M., et al. (2006), A review of present techniques and methodological advances in analyzing ^{234}Th in aquatic systems, *Mar. Chem.*, *100*, 190–212, doi:10.1016/j.marchem.2005.10.012.

Salter, I., R. S. Lampitt, R. Sanders, A. Poulton, A. E. S. Kemp, B. Boorman, K. Saw, and R. Pearce (2007), Estimating carbon, silica and diatom export from a naturally fertilised phytoplankton bloom in the Southern Ocean using PELAGRA: A novel drifting sediment trap, *Deep Sea Res., Part II*, *54*, 2233–2259, doi:10.1016/j.dsr2.2007.06.008.

Salter, I., A. E. S. Kemp, C. M. Moore, R. S. Lampitt, G. A. Wolff, and J. Holtvoeth (2012), Diatom resting spore ecology drives enhanced carbon export from a naturally iron-fertilized bloom in the Southern Ocean, *Global Biogeochem. Cycles*, *26*, GB1014, doi:10.1029/2010GB003977.

Savoye, N., K. O. Buesseler, D. Cardinal, and F. Dehairs (2004), ^{234}Th deficit and excess in the Southern Ocean during spring 2001: Particle export and remineralization, *Geophys. Res. Lett.*, *31*, L12301, doi:10.1029/2004GL019744.

Savoye, N., T. W. Trull, S. H. M. Jacquet, J. Navez, and F. Dehairs (2008), ^{234}Th-based export fluxes during a natural iron fertilization experiment in the Southern Ocean (KEOPS), *Deep Sea Res., Part II*, *55*, 841–855, doi:10.1016/j.dsr2.2007.12.036.

Smetacek, V. S. (1985), Role of sinking in diatom life-history cycles: Ecological, evolutionary and geological significance, *Mar. Biol.*, *84*, 239–251.

Smetacek, V., and S. W. A. Naqvi (2008), The next generation of iron fertilization experiments in the Southern Ocean, *Philos. Trans. R. Soc. A.*, *366*, 3947–3967.

Smetacek, V., et al. (2012), Deep carbon export from an iron-fertilized Southern Ocean diatom bloom, *Nature*, *487*, 313–319, doi:10.1038/nature11229.

Thiele, S., B. M. Fuchs, N. Ramaiah, and R. Amann (2012), Microbial community response during the iron fertilization experiment LOHAFEX, *Appl. Environ. Microbiol.*, *78*, 8803–8812, doi:10.1128/AEM.01814-12.

Trull, T. W., S. G. Bray, S. J. Manganini, S. Honjo, and R. François (2001a), Moored sediment trap measurements of carbon export in the Subantarctic and Polar Frontal Zones of the Southern Ocean, south of Australia, *J. Geophys. Res.*, *106*, 31,489–31,509.

Trull, T. W., S. R. Rintoul, M. Hadfield, and E. R. Abraham (2001b), Circulation and seasonal evolution of polar waters south of Australia: Implications for iron fertilization of the Southern Ocean, *Deep Sea Res., Part II*, *48*, 2439–2466.

Wanninkhof, R. (1992), Relationship between wind speed and gas exchange over the ocean, *J. Geophys. Res.*, *97*, 7373–7382.

Zeebe, R. E., and D. Archer (2005), Feasibility of ocean fertilization and its impact on future atmospheric CO_2 levels, *Geophys. Res. Lett.*, *32*, L09703, doi:10.1029/2005GL022449.